Plasma Physics and
Controlled Fusion

PAPER • **OPEN ACCESS**

The role of laser chirp in relativistic electron acceleration using multi-electron gas targets

To cite this article: A Grigoriadis *et al* 2023 *Plasma Phys. Control. Fusion* **65** 044001

OPEN ACCESS
IOP Publishing
Plasma Physics and Controlled Fusion
Plasma Phys. Control. Fusion **65** (2023) 044001 (6pp)
https://doi.org/10.1088/1361-6587/acbb25

The role of laser chirp in relativistic electron acceleration using multi-electron gas targets

A Grigoriadis[1,2], G Andrianaki[1,3], M Tatarakis[1,4], E P Benis[2,*] and N A Papadogiannis[1,5,*]

[1] Institute of Plasma Physics and Lasers, Hellenic Mediterranean University, Rethymno, 74100, Greece
[2] Department of Physics, University of Ioannina, 45110 Ioannina, Greece
[3] School of Production Engineering and Management, Technical University of Crete, 73100 Chania, Greece
[4] Department of Electronic Engineering, Hellenic Mediterranean University, 73133 Chania, Greece
[5] Physical Acoustics and Optoacoustics Laboratory, Department of Music Technology & Acoustics, Hellenic Mediterranean University, 74100 Rethymnon, Greece

E-mail: mbenis@uoi.gr and npapadogiannis@hmu.gr

Received 3 December 2022, revised 24 January 2023
Accepted for publication 10 February 2023
Published 1 March 2023

Abstract

The role of multi-10 TW chirped laser pulses interacting with N_2 gas jet targets, as a test case for multi-electron targets, is experimentally examined. Complementary measurements using He gas jet targets, which are fully ionized well before the laser pulse peak, are also presented for comparison with the measurements for the multi-electron N_2 targets. It is found that for both gases positively chirped laser pulses accelerate electrons more efficiently compared to the Fourier transform-limited and negatively chirped pulses. Furthermore, multi-electron targets offer additional electron injection mechanisms for efficient electron acceleration as a function of the chirp, due to the dynamic ionization of inner-shell electrons near the peak of the laser pulse. Finally, we show that the background plasma density value plays a critical role in the efficient acceleration of positively chirped pulses as well as in the tuning of the positive chirp value for maximizing the electron energy. We clearly observe that larger plasma density values require higher positive chirp values for efficient electron acceleration.

Keywords: laser wakefield acceleration (LWFA), laser plasma interaction, chirped laser pulses

(Some figures may appear in colour only in the online journal)

1. Introduction

The experimental demonstration of the laser wakefield acceleration process (LWFA) [1–3] has been one of the most important landmarks in the evolution of plasma physics and particle accelerator science. Recently, several university scale laboratories have implemented LWFA setups in their research arsenal, thus providing secondary sources of relativistic electron beams [4–7], exploited in basic research and applications, such as the generation of anti-matter [8], fuel ignition for inertial confinement fusion [9, 10], and radiation dosimetry [11]. Moreover, along with the relativistic electrons, betatron-type x-rays are produced [12–14], suitable for ultra-fast imaging [15, 16].

* Authors to whom any correspondence should be addressed.

Over the past two decades, significant effort was devoted to the study of the dynamics of the LWFA process, in an effort to harness it by controlling the electron injection mechanisms, either by the laser pulse characteristics [17–21] or the gas target species and geometry [22–25]. Currently, the daily basis controlled operation of a LWFA relativistic electron beam source, considering its maximum energy, energy spread, total charge and divergence is still an ongoing task. Additionally, the reproducibility of the electron beam should always be considered vital for certain applications [26], especially for radiotherapy [27].

Recently, we reported on a study about the dynamics of the LWFA electron acceleration using ultra-intense chirped laser pulses interacting with He gas targets [28]. In that study, it was shown that the use of positively chirped laser pulses improved the electron acceleration efficiency and provided more energetic electron beams. In this study, we extend our recent work to include multi-electron gas targets (N_2). Multi-electron gas targets are not fully ionized by the leading edge of the laser pulse, as for example He targets, and thus offer additional electron injection mechanisms that affect the outcome of the accelerated electron beams. In order to expose their role, we compare the relativistic electron spectra obtained from N_2 and He, using identically chirped laser pulses. To our knowledge, studies that involve chirped laser pulses and multi-electron targets are scarce in the literature. Thus, our work is a step toward such studies that are necessary for studying, improving and controlling the characteristics of the LWFA accelerated electron beams.

2. Experimental method

The experimental setup, developed at the Institute of Plasma Physics & Lasers [29] of the Hellenic Mediterranean University, has been recently described in detail in [28]. A simplified layout is shown in figure 1. The acceleration of the relativistic electron beams was driven by the 45 TW laser system 'Zeus,' delivering laser pulses with a maximum energy of $E = 1.3$ J at $R = 10$ Hz repetition rate, a central wavelength of $\lambda = 807$ nm, and a duration of $\tau = 24$ fs measured for the Fourier transform-limited (FTL) pulses. The contrast ratio of the laser pulses was measured to be 10^{-11} at 100 ps before the peak of the laser pulse [30]. The linear temporal chirp value of the laser pulse was set by a computer-controlled acousto-optic dispersive programmable filter (Fastlite Dazzler). Specifically, this filter modifies the chirp parameter a in the overall frequency of the laser pulse, $\omega = \omega_0 + at$, where ω_0 is the central angular frequency of the laser pulse. The laser beam is delivered to the experimental chamber where it is focused by an $f = 1$ m focal length parabolic mirror ($f/18$) to the gas-jet target area, thus resulting in a focal spot of 30 μm in diameter. Considering a measured pulse energy at the target of $E = 826$ mJ, a peak intensity of $I = (1.05 \pm 0.02) \times 10^{19}$ W cm^{-2} for the FTL pulses is reached. This peak intensity value corresponds to a normalized vector potential amplitude value of $a_0 = 2.2$.

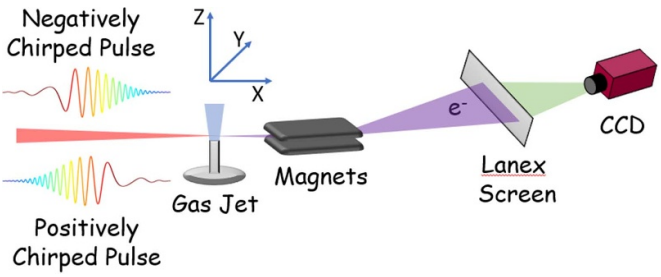

Figure 1. Layout of the experimental setup.

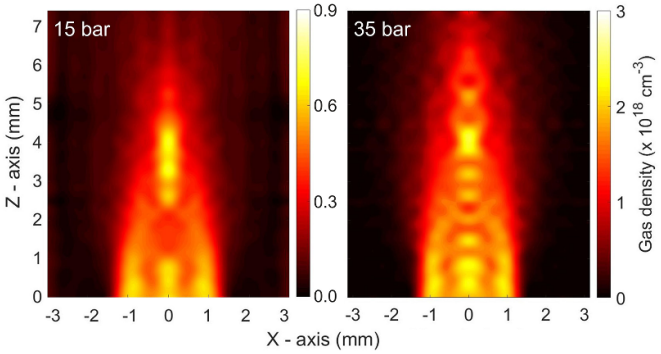

Figure 2. Interferometric measurements of the gas target density profiles of 15 and 35 bar backing pressure corresponding to N_2 and He, respectively.

The gas-jet flow was controlled by a pulsed electromagnetic valve, driven by the repetition rate of the laser. The gas valve was equipped with a home-made conical nozzle with a 3 mm in diameter exit hole. For the He gas, the backing pressure was optimally set at 35 bar. For the N_2 gas, the backing pressure was set at 15 bar, so that the resulting plasma electron density would be similar for both gases. The density profiles were accurately characterized using a Nomarski-type interferometer [30]. In figure 2 we present the measured two-dimensional gas density profiles for the two targets.

Thus, the average gas densities of 2×10^{18} cm^{-3} and 0.5×10^{18} cm^{-3}, measured at a distance of 1 mm above the exit hole of the nozzle, were determined for He and N_2 gas targets, at backing pressures of 35 and 15 bar, respectively. The He target contributes to the electron plasma density with two electrons, ionized by the leading edge of the laser pulse. On the other hand, the N_2 target contributes up to ten electrons for laser intensities up to 2×10^{16} W cm^{-2}, i.e. at the leading edge of the laser pulse well before the peak [14]. Considering the above, the resulting plasma electron densities for He and N_2 targets are 4×10^{18} cm^{-3} and 5×10^{18} cm^{-3}, respectively.

The energy spectra of the accelerated relativistic electrons were obtained using a magnetic spectrometer consisting of a pair of magnetic parallel plates, a scintillating screen (Lanex Regular) and a charge-coupled device (CCD) camera (see [30] for details). The electron spectrometer geometry and magnetic strength allowed for measuring electron spectra with energies higher than 60 MeV. The energy calibration of the spectra was based on home developed algorithms. Finally, the estimation

of the total number of electrons for each pixel of the CCD camera was determined from the independent calibration of the screen imaging system [30].

3. Results and discussion

In our recent work reported in [28], it was shown that there is an overall improvement of the acceleration efficiency of a relativistic electron beam, with respect to the maximum electron energy and current, by introducing a positive linear chirp to the laser pulses. Specifically, it was found that optimum conditions were reached by setting the chirp parameter to $+400\,\mathrm{fs}^2$, which corresponds to a laser pulse having duration of 60 fs measured at full width half maximum (FWHM). Here, we extend our chirp dependent investigations by including the N_2 gas as a multi-electron target, and thus introducing multiple ionization and related electron injection mechanisms in our study.

Specifically, we initially optimized the electron acceleration conditions (gas pressure, focusing geometry with respect to the gas jet, pulse jet timing, laser pulse energy) for He targets and for the FTL laser pulses. We then proceeded to the chirp dependent measurements for He targets by maintaining the same conditions as for the FTL pulses. However, for the N_2 targets we reduced the gas density from 35 to 15 bar in order to achieve almost equal plasma electron density to that of the He target, as mentioned above. The equality in the electron plasma density for both targets is critical for our study, since in this way, we fix one very sensitive experimental parameter and safely vary only the chirp of the pulse in an attempt to investigate the role of multi-electron targets in the electron acceleration via chirped laser pulses.

In figure 3, we present relativistic electron spectra for the He and N_2 gas targets in comparison with those obtained for FTL and positively chirped laser pulses. Three typical spectra are included for each chirp value depicting their repeatability. The He case shows a gradual smooth increase in the maximum electron energy that peaks at the chirp value of $400\,\mathrm{fs}^2$, beyond which a smooth decrease follows. No electron spectra were recorded for negatively chirped pulses. Possibly, in the latter case, the electrons were accelerated to energies lower that 60 MeV, which was our lower energy detection limit. The physics behind this chirp dependence has been detailed in [28]. In short, we showed that, for the few-10 TW pulses, positively chirped pulses result in the formation of smoother in structure plasma bubbles that favor electron injection at the rear end of the bubble, and thus result in higher maximum electron energies, as compared to the FTL and negatively chirped cases.

For the N_2 targets positively chirped pulses are seen to result in a maximization of the maximum electron energy for the laser chirp value of $500\,\mathrm{fs}^2$, $100\,\mathrm{fs}^2$ larger than in the case of He. Additionally, for near FTL laser pulses, N_2 shows a relatively higher maximum electron energy compared to He. It is worth mentioning that the electron spectra of N_2 show larger angular divergence compared to those of He, in accordance with similar results reported in [14]. In order to quantify the intrinsic differences in the maximum electron energies between He and N_2 targets, we determined their value for each spectrum at 25% of the maximum charge in the high energy tail of the spectrum. The dependence of the average maximum electron energy, corresponding to the spectra shown in figure 3, as a function of the laser chirp is presented in figure 4.

As clearly seen in figure 4, for N_2 targets near FTL pulses result in higher maximum energy than for He targets. This can be attributed to the additional electrons that are injected into the plasma bubble by the mechanism of ionization injection, which is initiated by the high peak intensity FTL pulses. Specifically, the L-shell electrons of nitrogen are ionized at laser intensities up to $2 \times 10^{16}\,\mathrm{W\,cm^{-2}}$, i.e., at the leading edge of the laser pulse well before the peak [28, 31]. These electrons form the background plasma, where a high intensity laser pulse propagates forming a plasma bubble, thus playing the same role as the K-shell electrons of He. Moreover, the K-shell electrons of nitrogen can be ionized either by tunneling or over the barrier ionization mechanisms at laser intensities around $1 \times 10^{19}\,\mathrm{W\,cm^{-2}}$, which is the case for the near FTL pulses in use. These K-shell electrons contribute to the direct ionization injection inside the bubble at the early stage of its formation, and thus finally result in accelerated electrons at relatively higher energies compared to those of He targets, where this mechanism is absent.

At a laser chirp value of $200\,\mathrm{fs}^2$ the maximum electron energy suffers a drop. Considering that the corresponding laser duration was measured 30 fs, the laser peak intensity is $8 \times 10^{18}\,\mathrm{W\,cm^{-2}}$, which is not adequate to support appreciable tunneling or over the barrier ionization of nitrogen K-shell electrons. Thus, the direct injection ionization mechanism is no longer supported and the maximum electron energy is attributed only to self-injection. In this case, the maximum electron energy for N_2 targets is about the same with that of He targets. However, for N_2 targets and larger laser chirp values, even though the laser intensity is further reduced, the maximum electron energy increases up to the laser chirp value of $500\,\mathrm{fs}^2$. For laser chirp values higher than $500\,\mathrm{fs}^2$ a large decrease in the maximum electron energy is evident. Moreover, laser pulses with negative chirp values did not result in measurable signals above the 60 MeV detection limit, as in the case of He targets.

From figure 4 it is evident that for N_2 targets, aside from the higher maximum energy values at FTL and $100\,\mathrm{fs}^2$ chirped laser pulses, there is an overall shift of the distribution of the maximum electron energy observed for He targets to higher laser chirp values. This behavior can be mainly attributed to the difference in the background plasma electron densities between He and N_2 targets, with the N_2 density measured to be 25% higher.

The above behavior can be understood considering that the maximum electric field amplitude, just before the electron density wave breaking occurs, is directly associated to the plasma bubble velocity, and described by the formula [32]:

$$E_{\max} = \frac{m_e c \omega_p}{e} \sqrt{2(\gamma - 1)}, \tag{1}$$

where m_e and e are the electron mass and charge, respectively, ω_p is the plasma frequency, and $\gamma = (1 - (u/c)^2)^{-1}$ is the

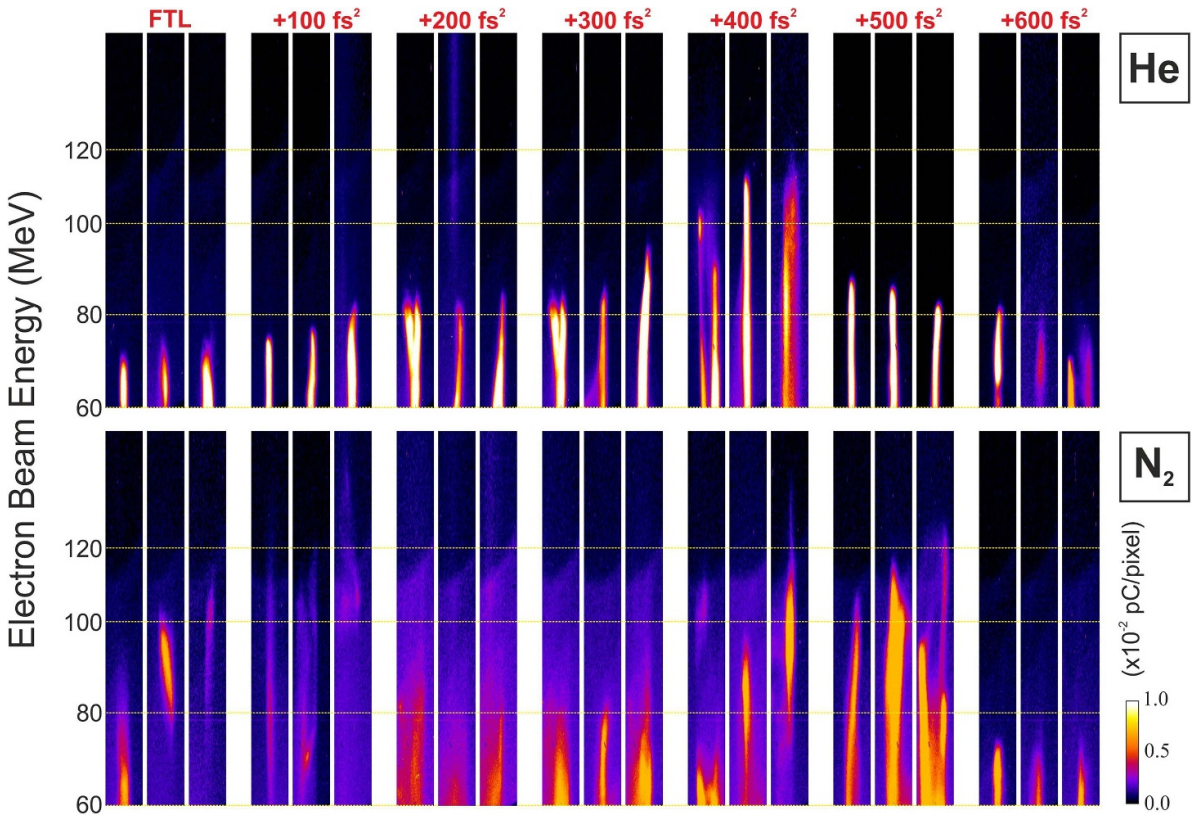

Figure 3. Relativistic electron spectra obtained after the interaction of FTL and chirped laser pulses with He and N_2 gas targets, respectively. The backing pressures for both gases were set so that they result in the same plasma electron density. Three spectra are shown for each chirp case to account for their repeatability.

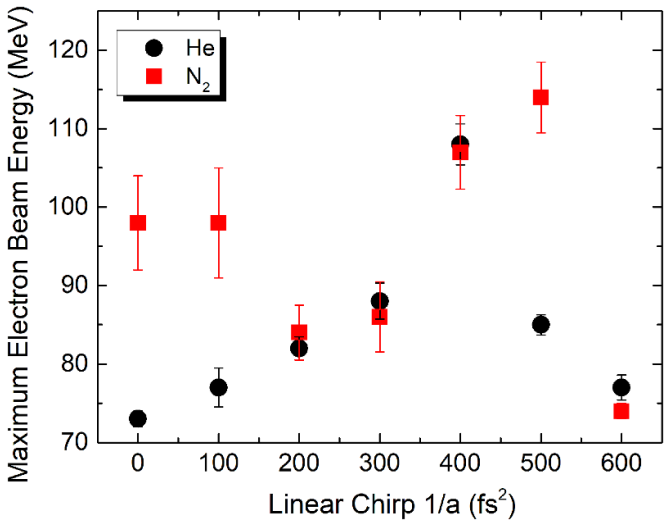

Figure 4. Maximum electron beam energy as a function of the laser pulse chirp for He (black filled circles) and N_2 (red filled squares) gas targets. The values were obtained for the spectra shown in figure 3. The error bars shown are statistical.

relativistic Lorentz factor. In addition, in the LWFA picture, the plasma bubble velocity is roughly equal to the group velocity, u_g, of a chirped laser pulse that propagates through the ionized medium, which is described as [28, 33]:

$$\frac{u_g}{c} = 1 - \frac{3}{2}\frac{\omega_p^2}{[\omega_0 \pm a(t-t_0)]^2}, \tag{2}$$

where ω_0 is the laser central frequency, a is the chirp parameter and t_0 the time corresponding to the peak of the pulse. Note that the chirp values, given in units of fs^2, correspond to the reciprocal of the chirp parameter, i.e. $1/a$.

Equation (2) indicates that positively chirped pulses, which have smaller group velocities than negatively chirped pulses, are expected to allow for a wavebreaking at lower electric field amplitude values compared to the ones corresponding to the negatively chirped pulses. The optimum conditions are reached for a certain chirp value, which for He is 400 fs^2. Assuming that these general optimum conditions are met also for N_2 targets, any variations should result only from the difference in the background plasma density. Then, according to equation (2), a 25% increase in the plasma density, which corresponds to an equal increase in the square of the plasma frequency, ω_p^2, should be matched by an increase in the chirp parameter a, so that the optimum group velocity u_g remains unaffected. This assumption is in accordance with the observed shift in the maximum electron energy shown in figure 4.

To further validate this argument, we obtained additional measurements of the electron spectra for He at a higher backing pressure of 50 bar. In figure 5, we present the

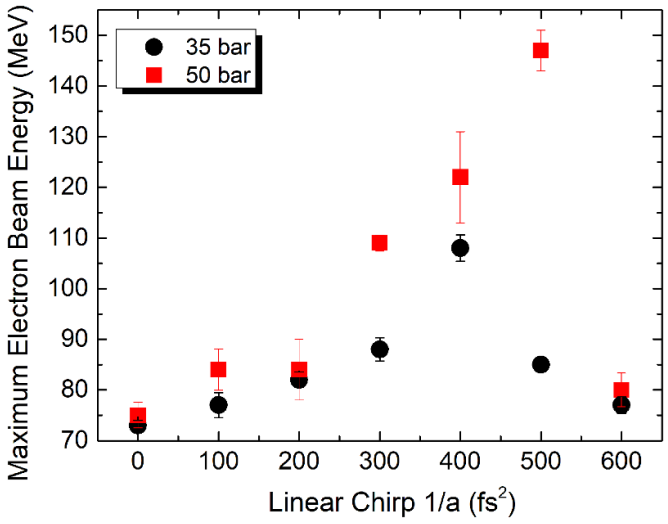

Figure 5. Maximum electron beam energy as a function of the laser pulse chirp for He targets at 35 bar (black filled circles) and 50 bar (red filled squares) backing pressures. The error bars shown are statistical.

measurements of the maximum electron beam energy as a function of the laser pulse chirp for He targets at 35 bar and 50 bar backing pressures, respectively. Interferometric measurements at 50 bar showed an increase in the plasma density of about 30%. This change shifts the optimum maximum electron energy to higher chirp values, thus corroborating a similar result for the N_2 case. Finally, it is worth mentioning that collisional ionization and dephasing effects can be safely excluded based on predictions from analytical calculations.

4. Conclusions

In this work, we have studied the role of multi-10 TW power laser chirped pulses in LWFA electron acceleration by comparing multi-electron N_2 targets with He targets. We experimentally demonstrate that positively chirped pulses, even though having lower peak intensities could favorably accelerate electrons at higher maximum energies compared to the FTL and negatively chirped pulses. The value of the positive chirp for the optimum maximum electron energy is directly connected to the background plasma density of the target. Larger plasma density requires higher positive chirp values for efficient electron acceleration. Furthermore, the mechanism of direct ionization injection of inner-shell electrons in multi-electron targets, that proceeds at appropriate laser peak intensities and laser chirp values, also contributes to the efficient electron acceleration resulting in relatively high maximum electron energies.

Data availability statement

The data that support the findings of this study are available upon reasonable request from the authors.

Acknowledgments

We acknowledge the valuable help of Dr Eugene Clark in the initial preparing of the electron acceleration setup prior to these experiments, Assist. Prof. Ioannis Fitilis and Mr Stylianos Petrakis for their support in running the ZEUS laser system. A G acknowledges financial support by the Hellenic Foundation for Research and Innovation (HFRI) under the 3rd Call for HFRI PhD Fellowships (Fellowship Number: 5985). This work has been carried out within the framework of the EUROfusion Consortium, funded by the European Union via the Euratom Research and Training Programme (Grant Agreement No. 101052200–EUROfusion) and the Hellenic National Program of Controlled Thermonuclear Fusion. Views and opinions expressed are however those of the author only and do not necessarily reflect those of the European Union or the European Commission. Neither the European Union nor the European Commission can be held responsible for them. The involved teams have operated within the framework of the Enabling Research Project: ENR-IFE.01.CEA-02 'Advancing shock ignition for direct-drive inertial fusion'.

ORCID iDs

A Grigoriadis https://orcid.org/0000-0002-5459-9288
M Tatarakis https://orcid.org/0000-0003-4285-3784
E P Benis https://orcid.org/0000-0002-5564-153X
N A Papadogiannis https://orcid.org/0000-0003-0691-2468

References

[1] Mangles S P *et al* 2004 *Nature* **431** 535–8
[2] Geddes C, Toth C, Van Tilborg J, Esarey E, Schroeder C, Bruhwiler D, Nieter C, Cary J and Leemans W 2004 *Nature* **431** 538–41
[3] Faure J, Glinec Y, Pukhov A, Kiselev S, Gordienko S, Lefebvre E, Rousseau J P, Burgy F and Malka V 2004 *Nature* **431** 541–4
[4] Leemans W P, Nagler B, Gonsalves A J, Tóth C, Nakamura K, Geddes C G, Esarey E, Schroeder C and Hooker S 2006 *Nat. Phys.* **2** 696–9
[5] Hafz N A *et al* 2008 *Nat. Photon.* **2** 571–7
[6] Kneip S *et al* 2009 *Phys. Rev. Lett.* **103** 035002
[7] Gonsalves A *et al* 2019 *Phys. Rev. Lett.* **122** 084801
[8] Sarri G *et al* 2013 *Phys. Rev. Lett.* **110** 255002
[9] Atzeni S *et al* 2022 *Europhys. News* **53** 18–23
[10] Atzeni S, Batani D, Danson C N, Gizzi L A, Perlado M, Tatarakis M, Tikhonchuk V and Volpe L 2021 *High Power Laser Sci. Eng.* **9** e52
[11] Labate L *et al* 2020 *Sci. Rep.* **10** 1–11
[12] Rousse A *et al* 2004 *Phys. Rev. Lett.* **93** 135005
[13] Corde S, Phuoc K T, Lambert G, Fitour R, Malka V, Rousse A, Beck A and Lefebvre E 2013 *Rev. Mod. Phys.* **85** 1
[14] Grigoriadis A, Andrianaki G, Tatarakis M, Benis E P and Papadogiannis N A 2021 *Appl. Phys. Lett.* **118** 131110
[15] Cole J *et al* 2015 *Sci. Rep.* **5** 1–7
[16] Hussein A E *et al* 2019 *Sci. Rep.* **9** 1–13
[17] Faure J, Rechatin C, Norlin A, Lifschitz A, Glinec Y and Malka V 2006 *Nature* **444** 737–9

[18] Kim H T *et al* 2017 *Sci. Rep.* **7** 1–8
[19] Shin J *et al* 2018 *Plasma Phys. Control. Fusion* **60** 064007
[20] Mohammed J, Ghotra H S, Kaur R, Hafeez H Y and Kant N 2017 *AIP Conf. Proc.* **1860** 020013
[21] Ghotra H S 2022 *Optik* **260** 169080
[22] McGuffey C *et al* 2010 *Phys. Rev. Lett.* **104** 025004
[23] Mirzaie M *et al* 2015 *Sci. Rep.* **5** 1–9
[24] Faure J, Rechatin C, Lundh O, Ammoura L and Malka V 2010 *Phys. Plasmas* **17** 083107
[25] Hansson M, Aurand B, Davoine X, Ekerfelt H, Svensson K, Persson A, Wahlström C G and Lundh O 2015 *Phys. Rev. Accel. Beams* **18** 071303
[26] Maier A R *et al* 2020 *Phys. Rev.* X **10** 031039
[27] Roa D, Kuo J, Moyses H, Taborek P, Tajima T, Mourou G and Tamanoi F 2022 *Photonics* **9** 2304–6732
[28] Grigoriadis A, Andrianaki G, Tazes I, Dimitriou V, Tatarakis M, Benis E P and Papadogiannis N A 2023 *Sci. Rep.* **13** 2918
[29] Clark E L *et al* 2021 *High Power Laser Sci. Eng.* **9** e53
[30] Grigoriadis A, Andrianaki G, Fitilis I, Dimitriou V, Clark E I, Papadogiannis N A, Benis E P and Tatarakis M 2022 *Plasma Phys. Control. Fusion* **64** 044007
[31] Fill E E 1994 *J. Opt. Soc. Am. B* **11** 2241–5
[32] Akhiezer A I and Polovin R 1956 *Sov. Phys. JETP* **3** 696–705
[33] Decker C and Mori W 1994 *Phys. Rev. Lett.* **72** 490